

Profile and Transport Studies in the outer Scrape Off Layer at ASDEX Upgrade

H.W. Müller, V. Bobkov, G. Haas, M. Jakobi, M. Laux, M. Maraschek, J. Neuhauser, M. Reich, V. Rohde, J. Schweinzer, E. Wolfrum, and ASDEX Upgrade Team
 MPI für Plasmaphysik, EURATOM-Association, D-85748 Garching, Germany

Introduction

The tokamak scrape off layer (SOL) shows typically a density wing which is thought to be related to quasi-macroscopic $E \times B$ edge turbulence on various space and time scales characterised by filamentary structures with preferential outward drift [1]. Such intermittent transport events are currently studied in several tokamak devices [2,3,4]. At ASDEX Upgrade a variety of edge diagnostics is available for the determination of accurate time averaged profiles as well as for the identification of fast transport events. As an extension of [1] we present here more recent results on these issues with focus on bottom single null H-mode discharges.

Experimental set up

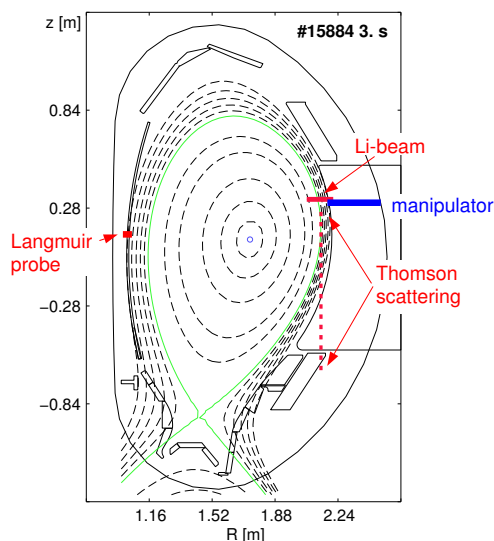


Figure 1: Poloidal cross section of ASDEX Upgrade with a set of diagnostics for density measurements.

Figure 1 shows the poloidal cross section of ASDEX Upgrade with the divertor IIb and the positions of the diagnostics for the density measurements presented in this paper. The green line indicates the separatrix for the discharge # 15884 which will be discussed later on, the black lines represent flux surfaces.

The Thomson scattering system [5] consists of six lasers which are passing the plasma vertically. The scattered light is observed at 16 vertically staggered positions. Each laser can be operated with a repetition rate of 20 Hz. The system can be operated with constant time distances or in burst mode with a time distance down to 100 ns between the six lasers. The single laser pulse length is 20 ns.

Another standard density diagnostic is the

Li-beam which is injected into the plasma at $z = 0.32$ m [6,7]. The density profiles are determined from lithium impact excitation spectroscopy (LIXS) [8]. While the Thomson scattering system delivers a snap shot of the density profiles the Li-beam profiles are always time integrated (usually 20 ms).

At nearly the same poloidal position ($z = 0.31$ m) a manipulator is available which can be operated with Langmuir probes [9]. We used a setup of four probe pins, two pairs consisting of one single probe and one floating potential measurement each. The two probe pairs were radially shifted by 4 mm. Another probe tip used as single probe is

mounted at the inner heat shield ($z = 0.13$ m). The Langmuir probe data were sampled with 500 kHz.

Edge density profiles

On the left side of figure 2 the density profile is shown for discharge #12200, which had been analysed in some detail in [1] (plasma current $I_P = 1$ MA, magnetic field $B_t = -2.5$ T, safety factor $q \approx 5$, line averaged density $n_e = 8.5 \times 10^{19} \text{ m}^{-3}$, fraction of Greenwald density $n_e/n_{GW} \approx 0.67$, neutral beam heating power $P_{NI} = 5$ MW, neutral gas flux in the main chamber $\Gamma_0 = 10^{21} \text{ m}^{-2} \text{ s}^{-1}$, medium triangularity). There is a very steep gradient around the separatrix and the gradient length λ_n (about 0.9 cm) is about constant across the separatrix indicating a transport correlation across the separatrix. This region shows rather stiff profiles indicating ballooning and drift mode characteristics [1]. About 1 cm outside the separatrix, but still far from the limiter, the profile becomes much flatter ($\lambda_n \approx 5$ cm). It was shown that transport in this SOL wing is well above Bohm diffusion [1]. In the following we discuss these issues for discharge #15884, which has much lower density and for which we have looked for transient events in some detail as described in the next section. The parameters of this discharge were $I_P = 800$ kA, $B_t = -2.0$ T, $q \approx 4.0$, $n_e = 3.7 \times 10^{19} \text{ m}^{-3}$, $n_e/n_{GW} \approx 0.37$, $P_{NI} = 5$ MW, $\Gamma_0 = 4 \times 10^{20} \text{ m}^{-2} \text{ s}^{-1}$, low triangularity, without gas puffing.

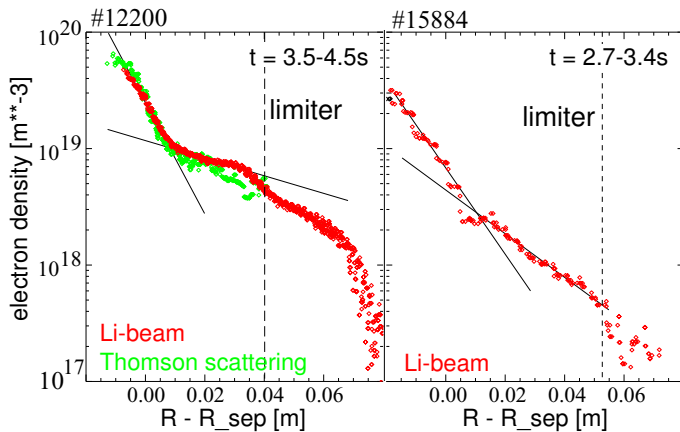


Figure 2: Edge density profiles measured by the Li-beam and Thomson scattering system in various discharges. The profiles are averaged by a median. The solid black lines represent the gradients around the separatrix and in the cold SOL. The vertical broken black lines indicate the position of a limiter affecting the Li-beam profiles.

Just like #12200, this discharge shows a steep gradient around the separatrix and a density wing in the SOL, though with much faster decay. The gradient lengths are $\lambda_n = 1.1$ cm around the separatrix and 2.2 cm in the outer SOL. A comparison between density profiles including ELMs and excluding ELM periods indicate that the profile flattening is not caused by ELMs.

Combining the density profile with the measured recycling flux Γ_0 and following the procedure outlined in [1], we get a radially increasing average outward transport velocity of $v_{out} \approx 100 \text{ ms}^{-1}$ and 250 ms^{-1} at $R - R_{sep} = 2$ and 4 cm. These values are corresponding to a formal diffusion coefficient $D_{\perp} = 2.2$ and $5.5 \text{ m}^2 \text{ s}^{-1}$, again much larger than the Bohm diffusion coefficient ($D_B = 0.3 \text{ m}^2 \text{ s}^{-1}$ for a typical SOL temperature of 10 eV). Possible candidates for such a quasi-macroscopic filamentary transport are discussed in e.g. in references [1-4,10] and also in the next section.

Macroscopic transport events in the scrape off layer

Discharge # 15884 shows very strong events on the Langmuir probes when the manipulator probes were sited 3.6 – 4.0 cm behind the limiter. The ion saturation current was not measured continuously since the probes were operated as single probes. Figure 4 shows the time traces of the floating potential and the ion saturation current seen by

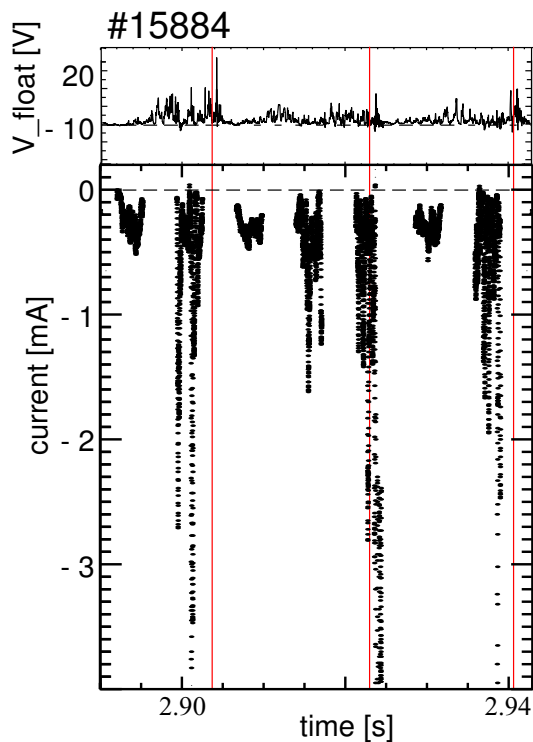


Figure 4: Bursts and fluctuation activity of a Langmuir probe's floating potential (top) and the ion saturation current (bottom) rise before ELM events.

the probe tips closer to the separatrix (named pair 1). The red vertical lines indicate the onset of ELMs. After an ELM event there is a quiet period of < 10 ms seen in the floating potential. Then the potential starts to fluctuate until the next ELM starts. The same behaviour can be seen in the ion saturation current. The first period of ion saturation measurements in between ELMs shows only a weak signal variation while the second period shows strong bursts. Some of the bursts in the last 5 ms before an ELM show an enhancement of the current by more than a factor of 10. The following figure shows the measurements in more detail. On the left hand side the measurements during a type I ELM are shown and on the right hand side the measurements during the period after an ELM. On both sides from top to bottom the following time traces are shown: D_α signal in the outer divertor (green), signal indicating mode activity from magnetic measurements (blue), floating potential of tip pair 2 (red),

floating potential of tip pair 1 (black), and the according ion saturation currents. The left picture shows that before the ELM onset the floating potentials show fluctuations. Also the ion saturation currents show bursts correlated with floating potential changes in the 1 – 2 V range. Then at 3.0677 s the ELM crash starts which is seen in all signals at once. For the first 200 μ s the floating potential is strongly and fast oscillating. Then a burst-like structure occurs. Also the currents show strong oscillations at the beginning of the ELM. After about 500 μ s several strong bursts can be seen in the current signals. At the same time bursts are seen in the floating potential. The ELM activity ends after about 3 ms. Additional information can be drawn from the Thomson scattering system in another discharge. This system detects burst-like density and correlated temperature enhancements in the early phase of an ELM in the steep gradient zone. Additionally density events in the SOL were detected. These events are poloidally localised [5]. Temperature measurements by an electron cyclotron emission diagnostic also show oscillations before the ELM crashes [11].

On the right hand picture the D_α signal indicates that an ELM just finished at 2.942 s. The ion saturation current shows small bursts again 2 ms after the ELM which can also be seen in the floating potentials. At $t = 2.951$ s once more two very strong

bursts are seen clearly in the saturation currents. Also the floating potential is changing. The magnetic probes and the D_α signal in the divertor do not see these events.

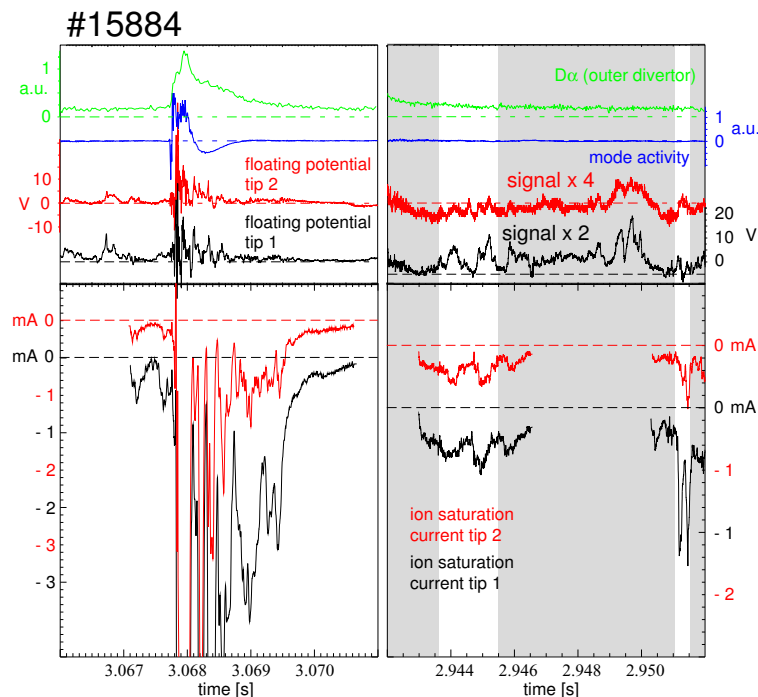


Figure 5: Transport events observed by a Langmuir probe. Left hand side floating potential and current measurement during an ELM. On the right hand side transport events in between ELMs.

The probe at the inner heat shield is directly connected to the low field side by the magnetic field. Nevertheless in between and before ELMs there is no evidence for such filamentary transport events in the ion saturation current as seen at the low field side. ELM crashes can be observed at the high field side. In between ELMs the signal's variation stays almost unchanged while the average saturation current is decreasing.

Summary and conclusions

Density profiles in H-mode discharges always show a wing in the cold SOL which cannot be explained by transport due to small scale electrostatic turbulence. A possible explanation is the existence of filamentary transport driven by ballooning or drift mode instabilities in the SOL itself on a centimetre scale length. Burst-like transport events were observed close to the separatrix as well in the far SOL and even in the limiter shadow. These events were seen in between ELMs especially before the onset of ELM crashes. The observed strong variations during ELMs were expected. Though transient events have been identified in various discharge scenarios, a statistical analysis has not been done yet.

References

- [1] J. Neuhauser et al., *Plasma Phys. Contr. Fusion*, **44** 855 (2002)
- [2] B. LaBombard et al., *Nuclear Fusion*, **40** 2041 (2000)
- [3] S. Krasheninnikov, *Physics Letters A*, **283** 368 (2001)
- [4] D.L. Rudakov, *Plasma Phys. Contr. Fusion*, **44** 717 (2002)
- [5] M. Jakobi et al., *this conference* P1.122
- [6] S. Fiedler, IPP Report III/209 (1995)
- [7] H.W. Müller et al., *28th conf. on Controlled Fusion Fusion and Plasma Physics*, P1.109 (2001)
- [8] J. Schweinzer et al., *Plasma Phys. Contr. Fusion*, **34** 53 (1992)
- [9] V. Rohde et al., *J Nucl. Mater.*, **241-243** 712 (1997)
- [10] M. Endler et al., *Nucl. Fusion*, **35** 1307 (1995)
- [11] H. Zohm, *Plasma Phys. Contr. Fusion*, **38** 105 (1996)